AIAA JOURNAL
Vol. 42, No. 7, July 2004

Magnetohydrodynamic and Electrohydrodynamic Control of Hypersonic Flows of Weakly Ionized Plasmas

Sergey O. Macheret,* Mikhail N. Shneider,† and Richard B. Miles‡
Princeton University, Princeton, New Jersey 08544

The focus of this work is on theoretical analysis of fundamental aspects of high-speed flow control using electric and magnetic fields. The principal challenge is that the relatively cold gas is weakly ionized in electric discharges or by electron beams, with ionization fraction ranging from 10^{-8} to 10^{-5}. The low ionization fraction means that, although electrons and ions can interact with electromagnetic fields, transfer of momentum and energy to or from the bulk neutral gas can be quite inefficient. Analytical estimates show that, even at the highest values of the electric field that can exist in cathode sheaths of electric discharges, electrohydrodynamic, or ion wind, effects in a single discharge can be of significance only in low-speed core flows or in laminar sublayers of high-speed flows. Use of multi-element discharges would amplify the single-sheath effect, so that the cumulative action on the flow can conceivably be made significant. However, Joule heating can overshadow the cathode sheath ion wind effects. Theoretical analysis of magnetohydrodynamic (MHD) flow control with electron beam ionization of hypersonic flow shows that the MHD interaction parameter is a steeply increasing function of magnetic field strength and the flow velocity. However, constraints imposed by arcing between electrode segments can reduce the performance and make the maximum interaction parameter virtually independent of Mach number. Estimates also show that the MHD interaction parameter is much higher near the wall (in the boundary layer) than in the core flow, which may have implications for MHD boundary layer and transition control. The paper also considers "electrodeless" MHD turning and compression of high-speed flows. Computations of a sample case demonstrate that the turning and compression of hypersonic flow ionized by electron beams can be achieved; however, the effect is relatively modest due to low ionization level.

Nomenclature

B	=	magnetic field
B_z, B_r	=	z component and r component of the magnetic field
$B_a(z)$	=	local amplitude of B field on the z axis
$B_{a,\max}$	=	maximum value of the magnetic field
c_f	=	friction drag coefficient
E_{eff}	=	effective electric field
$\boldsymbol{E}^*$	=	electric field in the reference frame moving with the gas, $\boldsymbol{E}+\boldsymbol{u}\times\boldsymbol{B}$
E_a	=	electric field strength at the anode
E_c	=	Hall field corresponding to the arcing threshold
E_{cath}	=	electric field strength at the cathode
E_v, E_v^0	=	nonequilibrium and equilibrium values of vibrational energy per unit volume
E_φ^*	=	azimuthal electric field component in the reference frame moving with the gas
e	=	electron charge
e_{tot}	=	total energy (internal energy, excluding the energy of vibrational mode, plus kinetic energy) of the gas per unit volume
F_z, F_r	=	z component and r component of the $\boldsymbol{j}\times\boldsymbol{B}$ force
f, g	=	functions defined in Eq. (21)
H	=	column vector in Euler equations
$\dot{H}_{\text{inlet}}$	=	total enthalpy entering the inlet per unit time
h	=	flight altitude
$\hbar$	=	Planck's constant
$\boldsymbol{j}$	=	electric current density
j_b	=	current density of the beam at the injection point
j_φ	=	azimuthal current density component
k	=	load factor
k_d	=	rate coefficient of collisional detachment of electrons from negative ions
k_{e+}, k_{e-}, k_{en}, k_{+-}, k_{n+}, k_{n-}	=	rate coefficients of collisional momentum transfer between different kinds of particles
L	=	length of magnetohydrodynamic (MHD) region
L_R	=	electron beam relaxation length
M	=	Mach number
M_n	=	mass of an atom/molecule
M_+	=	positive ion mass
M_-	=	negative ion mass
m	=	mass of electron
$\dot{m}$	=	mass flow rate
N	=	number of consecutive elements (multiple discharges)
N_O	=	number density of oxygen atoms
n	=	number density of gas molecules
n_+, n_-, n_e	=	number densities of positive ions, negative ions, and electrons
p	=	static gas pressure
p_E	=	electric pressure
p_e	=	electron gas pressure
p_n	=	partial pressure of neutral particles
$\langle p_{\text{tot}}\rangle$	=	total pressure averaged over the inlet cross section
$p_{\text{tot},0}$	=	freestream total pressure
p_+	=	positive ion partial pressure

Presented as Paper 2002-2249 at the AIAA 33rd Plasmadynamics and Lasers Conference, Maui, HI, 20–23 May 2002; received 18 July 2003; revision received 8 December 2003; accepted for publication 8 March 2004.

*Senior Research Scientist, D-414 Engineering Quadrangle, Department of Mechanical and Aerospace Engineering; macheret@princeton.edu. Associate Fellow AIAA.

†Research Staff Member, D-414 Engineering Quadrangle, Department of Mechanical and Aerospace Engineering. Senior Member AIAA.

‡Professor, D-414 Engineering Quadrangle, Department of Mechanical and Aerospace Engineering. Fellow AIAA.

p_- = negative ion partial pressure
Q_b = total power deposited by the e-beam
Q_J = Joule dissipation rate
Q_v = power deposited per unit volume into vibrational excitation
Q_{VT} = heating rate per unit volume due to vibration-translation (VT) relaxation
q = dynamic pressure
q_b = power density deposited by the e-beam
q_i = ionization rate due to electron beam
R = column vector in Euler equations
Re_M = magnetic Reynolds number
Re_x^* = Reynolds number calculated at the reference temperature T^*
r = coordinate
r_{inlet} = inlet radius
$r_{\max}$ = maximal radius of the numerical domain
S = MHD interaction parameter (Stuart number)
S_τ = MHD interaction parameter with respect to shear stress at the wall
T = translational-rotational gas temperature
T_v = vibrational temperature
T^* = reference temperature
$\boldsymbol{U}$ = column vector in Euler equations
$\boldsymbol{u}$ = gas velocity
u_∞ = freestream velocity
u_z, u_r = z component and r component of the gas velocity
$\tilde{u}_r, \tilde{u}_z$ = effective electron-ion velocity components across magnetic field taking into account ion slip
u' = characteristic velocity in the near-wall region (friction velocity)
$\boldsymbol{V}_e, \boldsymbol{V}_+, \boldsymbol{V}_-, \boldsymbol{V}_n$ = convective velocities of electrons, positive ions, negative ions, and neutral atoms/molecules
$V_{\mathrm{dr}}^+, V_{\mathrm{dr}}^e$ = ion and electron drift velocities
W_i = energy cost of ionization, that is, the loss of electron beam energy per each newly generated electron in the plasma
x = coordinate
$\boldsymbol{Z}$ = column vector in Euler equations
Z_{EHD} = electrohydrodynamic (EHD) interaction parameter
Z_{tot} = total interaction parameter
Z_ε = ratio of Joule and viscous dissipation rates
Z_τ = EHD interaction parameter for the boundary layer
z = coordinate
z_{inlet} = inlet axial location
$z_{\max}$ = maximum length of the numerical domain
α = Townsend ionization coefficient
β = electron-ion recombination rate coefficient
β_{ii} = ion–ion recombination rate coefficient
$\boldsymbol{\Gamma}_e, \boldsymbol{\Gamma}_+, \boldsymbol{\Gamma}_-$ = fluxes of electrons, positive ions, and negative ions
γ = specific heat ratio
ε = work done on an electron by the induced Faraday electric field during the electron's lifetime with respect to dissociative recombination with ions
ε_b = initial energy of beam electrons
$\varepsilon_{\mathrm{int}}$ = internal energy (excluding the energy of vibrational mode) per unit mass
ε_0 = permittivity of free space
ζ = ratio of the ionization cost to the work done on an electron by the induced Faraday electric field during the electron's lifetime
η_v = fraction of the Joule dissipation rate spent on vibrational excitation of molecules
θ = turning angle of the flow
μ = dynamic viscosity
μ_0 = permeability of free space
ν_a = electron attachment frequency (i.e., the number of attachments per unit time)
ρ = gas density
ρ_∞ = freestream density
σ = scalar electrical conductivity
τ = shear stress at the wall
τ_{VT} = nitrogen vibrational relaxation time
φ = electric potential
Ω_e = electron Hall parameter
Ω_+ = ion Hall parameter

I. Introduction

THERE is a growing interest in using weakly ionized gases (plasmas) and electric and magnetic fields in high-speed aerodynamics. Wave and viscous drag reduction, thrust vectoring, reduction of heat fluxes, sonic boom mitigation, boundary-layer and turbulent transition control, flow turning and compression, onboard power generation, and scramjet inlet control are among plasma and MHD technologies that can potentially enhance performance and significantly change the design of supersonic and hypersonic vehicles.[1–30] Meanwhile, despite many studies devoted to these new technologies, a number of fundamental issues have not been adequately addressed. Any plasma created in gas flow and interacting with electric and magnetic fields would result in gas heating. This heating can certainly have an effect on the flow and, in some cases, can be used advantageously. However, a more challenging issue is whether significant nonthermal effects of plasma interaction with electric and magnetic fields can be used for high-speed flow control.

In conventional MHD of highly conducting fluid, electric and magnetic effects give rise to ponderomotive force terms $\nabla(\varepsilon_0 E^2/2)$ and $\nabla(B^2/2\mu_0)$, which can be interpreted as gradients of electric and magnetic field pressures. These ponderomotive forces are successfully utilized for plasma containment in fusion devices and also play an important role in astrophysics. One might hope that these forces can also be used for control of high-speed flow of ionized air. However, the great importance of ponderomotive forces in fusion and astrophysical plasmas is due to the fact that those plasmas are fully, or almost fully, ionized and, therefore, are highly conductive. In contrast, high-speed air encountered in aerodynamics is not naturally ionized, even in boundary layers and behind shocks if the flight Mach number is below about 12, due to the low static temperature. Therefore, ionization has to be created artificially, using various electric discharges or high-energy particle beams.[16,18,22–24,26–28,31–34] In most conditions, the artificially created plasmas are weakly ionized, with ionization fraction ranging from 10^{-8} to 10^{-5}. Because of the low ionization fraction and electrical conductivity, interaction of the plasma with electromagnetic fields and transfer of momentum and energy to or from the bulk neutral gas can be quite inefficient.

In the present paper, we derive analytical formulas for the so-called interaction parameters that characterize EHD and MHD effects on gas flows. Numerical estimates based on these formulas are then performed to determine the trends and ranges of conditions where EHD and MHD effects can be significant.

II. Theoretical Analysis of Magnetohydrodynamic and Electrohydrodynamic Effects in Weakly Ionized Gas Flows

A. Basic Equations

To analyze effects of electric and magnetic forces on weakly ionized gas flows, we denote number densities of electrons, positive and negative ions, and neutrals as n_e, n_+, n_-, and n; velocities as $\boldsymbol{V}_e$, $\boldsymbol{V}_+$, $\boldsymbol{V}_-$, and $\boldsymbol{V}_n$; and pressures as p_e, p_+, p_-, and p_n. Rate coefficients of collisional momentum transfer between different kinds of particles will be denoted k_{e+}, k_{e-}, k_{en}, k_{+-}, k_{n+}, and k_{n-}. Electric and magnetic fields are denoted as usual: $\boldsymbol{E}$ and $\boldsymbol{B}$. For simplicity, we will assume that masses of both positive and negative ions are equal to the mass of a neutral molecule, and any of those greatly exceeds the electron mass m: $M_+ = M_- = M_n \gg m$. Equations of motion for a four-fluid mixture are then

$$n_e \frac{d(m\boldsymbol{V}_e)}{dt} = -en_e(\boldsymbol{E} + \boldsymbol{V}_e \times \boldsymbol{B}) - \nabla p_e - k_{e+}n_e n_+ m(\boldsymbol{V}_e - \boldsymbol{V}_+) - k_{e-}n_e n_- m(\boldsymbol{V}_e - \boldsymbol{V}_-) - k_{\mathrm{en}} n_e n m(\boldsymbol{V}_e - \boldsymbol{V}_n) \tag{1}$$

$$n_+ \frac{d(M_n\boldsymbol{V}_+)}{dt} = en_+(\boldsymbol{E} + \boldsymbol{V}_+ \times \boldsymbol{B}) - \nabla p_+ - k_{e+}n_e n_+ m(\boldsymbol{V}_+ - \boldsymbol{V}_e) - k_{+-}n_+ n_- M_n(\boldsymbol{V}_+ - \boldsymbol{V}_-) - k_{n+} n_+ n M_n(\boldsymbol{V}_+ - \boldsymbol{V}_n) \tag{2}$$

$$n_- \frac{d(M_n\boldsymbol{V}_-)}{dt} = -en_-(\boldsymbol{E} + \boldsymbol{V}_- \times \boldsymbol{B}) - \nabla p_- - k_{e-}n_e n_- m(\boldsymbol{V}_- - \boldsymbol{V}_e) - k_{+-}n_+ n_- M_n(\boldsymbol{V}_- - \boldsymbol{V}_+) - k_{n-} n_- n M_n(\boldsymbol{V}_- - \boldsymbol{V}_n) \tag{3}$$

$$n \frac{d(M_n\boldsymbol{V}_n)}{dt} = -\nabla p_n - k_{\mathrm{en}} n_e n m(\boldsymbol{V}_n - \boldsymbol{V}_e) - k_{n+} n_+ n M_n(\boldsymbol{V}_n - \boldsymbol{V}_+) - k_{n-} n_- n M_n(\boldsymbol{V}_n - \boldsymbol{V}_-) + \mu \Delta \boldsymbol{V}_n \tag{4}$$

where μ is the dynamic viscosity. Adding these equations, we obtain a single-fluid equation containing the total density ρ, mass velocity $\boldsymbol{u}$, pressure $p = p_n + p_+ + p_- + p_e$, and electric current density $\boldsymbol{j} = e(n_+\boldsymbol{V}_+ - n_-\boldsymbol{V}_- - n_e\boldsymbol{V}_e)$:

$$\rho \frac{d\boldsymbol{u}}{dt} = -\nabla p + e(n_+ - n_- - n_e)\boldsymbol{E} + \boldsymbol{j} \times \boldsymbol{B} + \mu \Delta \boldsymbol{u} \tag{5}$$

Note that the viscous terms in Eqs. (4) and (5) are written for the simplest case of incompressible flow with constant viscosity, because the main focus is on interaction of charged species with electric and magnetic fields and with neutral molecules [the second and third terms on the right-hand side of Eq. (5)]. However, the resulting Eq. (5) can be easily written for the general case of compressible flow with variable viscosity: the well-known viscous terms of Navier–Stokes equations should be simply substituted for the last term on the right-hand side of Eq. (5).

B. Electrohydrodynamic, or "Ion Wind," Flow Control

Consider EHD effects first. These effects, alternatively referred to as "ion wind,"[35] are represented by the second term on the right-hand side of Eq. (5). The strength of the EHD effect is proportional to the net space charge density. Bulk plasmas are known to be quasi-neutral, that is, in them, $n_+ \simeq n_- + n_e$ with very good accuracy. Substantial EHD effects can be expected only in the presence of a significant space charge, which is the case in cathode sheaths or in space-charge regions of corona discharges. Having those space-charge regions or sheaths in mind, in what follows we will neglect n_- and n_e in comparison with n_+. The change in momentum of a gas element moving along the x axis through a space-charge region is $d(\rho u) = en_+E \cdot \mathrm{d}t = en_+E \cdot \mathrm{d}x/u$. Therefore, the relative strength of EHD effects can be characterized by a dimensionless EHD interaction parameter equal to the ratio of EHD push work to the fluid momentum flux:

$$Z_{\mathrm{EHD}} = en_+\Delta\varphi \big/ \rho u^2 \tag{6a}$$

where $\Delta\varphi = \int E\,\mathrm{d}x$ is the voltage fall across the space-charge region.

An alternative way of expressing EHD effects is to use the Poisson equation, which in a one-dimensional case can be written as $\mathrm{d}E/\mathrm{d}x = e(n_+ - n_- - n_e)/\varepsilon_0$. With the Poisson equation, the second term on the right-hand side of Eq. (5) can be transformed into

$$e(n_+ - n_- - n_e)E = \varepsilon_0 E \frac{\mathrm{d}E}{\mathrm{d}x} = \frac{\mathrm{d}}{\mathrm{d}x}\left(\frac{\varepsilon_0 E^2}{2}\right)$$

which can be interpreted as a gradient of the "electric pressure" $p_E = \varepsilon_0 E^2/2$. Therefore, in a one-dimensional flow between the anode and cathode of a glow discharge, the drop of electric pressure between the anode and cathode is

$$\Delta p_E = (\varepsilon_0/2)\left(E_{\mathrm{cath}}^2 - E_a^2\right)$$

where E_{cath} and E_a are the electric field strengths at the cathode and anode, respectively. In most cases, E_a is negligible compared with E_{cath} (Ref. 36). Thus, the EHD interaction parameter can be expressed as

$$Z_{\mathrm{EHD}} = \frac{en_+\Delta\varphi}{\rho u^2} = \frac{\Delta p_E}{\rho u^2} = \frac{\varepsilon_0 E_{\mathrm{cath}}^2}{2\rho u^2} \tag{6b}$$

Two principal examples of electric discharge systems that have substantial voltage drops across space-charge regions and may be used for EHD flow control are positive corona and the cathode sheath of a glow discharge.

In a positive corona in atmospheric air, n_+ can realistically reach about 10^8 cm^{-3}, and $\Delta\varphi$ can be from several kilovolts to several tens of kilovolts.[36] With $\Delta\varphi = 40$ kV, the interaction parameter Z_{EHD} will be at least 0.1 only for flows with very low dynamic pressure, 3 Pa or less. For standard sea-level air, this means that the flow velocity should be 2 m/s or lower.

In cathode sheaths of glow discharges, ion density can reach about 10^{11} cm^{-3} (Ref. 36). Cathode voltage fall in normal (low-current) glow discharges is about 200–300 V, and it can reach about 1 kV in abnormal (high-current) glow discharges.[36] Then, to make $Z_{\mathrm{EHD}} \geq 0.1$, the dynamic pressure should be less than 80 Pa, corresponding to the maximum flow velocity below 11.3 m/s in standard sea-level air, or below 35.8 m/s in air with one-tenth normal density. Note that effects of surface glowslike discharges with dielectric barrier on low-speed flows have been experimentally demonstrated.[37,38]

In principle, a stable discharge with electron density on the order of 10^{12}–10^{13} cm^{-3} can be maintained between the cathode and the anode in longitudinal airflow preheated to 2000–3000 K at a pressure of 1 atm (0.1013 MPa) (Ref. 39). In such systems, assuming that the temperature is 2400 K, the charge number density is 10^{12}–10^{13} cm^{-3}, and the cathode voltage fall is 1 kV; the EHD interaction parameter, according to Eq. (6a), can reach 1 at dynamic pressure of 800–8000 Pa, corresponding to flow velocities of 23–72 m/s.

An estimate of the maximum EHD effect can also be obtained with Eq. (6b). If thermal emission of electrons from the cathode is insignificant, so that electrons are emitted due to the ion and photon bombardment of the cathode and then multiply in the cathode sheath in Townsend avalanche processes, then the cathode electric field E_c can be very strong: $E_{\mathrm{cath}}/n \approx 10^{-14}\mathrm{V} \cdot \mathrm{cm}^2$ (Ref. 36). Therefore, for the highest value of Z_{EHD} in Eq. (6b), not only does the cathode sheath have to be dominated by Townsend processes, but the gas density should be as high as possible. If a Townsend cathode sheath could exist at normal atmospheric density, then the EHD interaction parameter would reach 1 at dynamic pressure of about 1600 Pa, corresponding to a flow velocity of about 50 m/s. At a density of one-tenth of standard sea-level atmospheric density, diffuse glow discharges in air with Townsend cathode sheaths certainly can exist; in that case, $Z \approx 1$ at a dynamic pressure of about 160 Pa, corresponding to a flow velocity of about 16 m/s.

Note that, when assessing EHD effects on specific gas flows, the fraction of a gas actually passing through the interaction region (i.e., through the cathode sheath) is as important as the interaction parameter for that fraction of the gas. Because at high pressures, where the interaction parameter can be relatively high, the cathode sheath thickness is micron-scale small, the EHD interaction can affect only a very small portion of the macroscopic flow.

Estimates in the previous paragraphs referred to freestream conditions. However, from Eqs. (6a) and (6b) it is clear that maximum EHD effects will occur where the flow velocity is the slowest, that is, in the boundary layer. For the boundary layer, the interaction parameter can be defined as the ratio of electrostatic and shear (friction) forces:

$$Z_\tau = en_+\Delta\varphi/\tau \tag{7}$$

where τ is the shear stress at the wall. This equation is essentially equivalent to Eq. (6a) where $\boldsymbol{u}$ is a characteristic velocity in the near-wall region, also called the friction velocity[40]: $\boldsymbol{u} = u'$, where $\rho u'^2 = \tau$, or

$$u' = \sqrt{\tau/\rho} \tag{8}$$

The wall shear stress can be related to freestream conditions ρ, u with well-known correlations[41]:

$$\tau = \frac{1}{2}\rho u^2 c_f \tag{9}$$

$$c_f = \frac{0.664}{\sqrt{Re_x^*}} \qquad \text{for laminar flow}$$

$$= \frac{0.0592}{\left(Re_x^*\right)^{0.2}} \qquad \text{for turbulent flow} \tag{10}$$

where Re_x^* is the Reynolds number calculated at the reference temperature T^*. Therefore,

$$Z_\tau = en_+\Delta\varphi\Big/\rho u^2 \times 2/c_f \tag{11}$$

and, since $c_f \ll 1$ for high-Reynolds-number flows, Z_τ greatly exceed Z. For example, in the range $Re_x^* = 10^5$–10^7, the factor $2/c_f \approx 10^3$, so that ion wind effects in the cathode sheath of a glow discharge may affect the boundary layer and skin friction in standard sea-level airflow whose velocity far from the surface is up to 114 m/s. In air with 0.1 normal density, the velocity limit increases to 360 m/s.

The estimates in the preceding paragraphs, using Eqs. (6a), (6b), and (7), assumed that a single cathode–anode pair is used for flow control. However, multiple discharges can be conceivably used, so that the cumulative effect of many cathode sheaths would affect the flow. A rough estimate of the number of consecutive elements, N, required to make the total interaction parameter $Z_{\text{tot}} \approx 0.1$–1, is simply $N = Z_{\text{tot}}/Z_{\text{EHD}}$ or $N = Z_{\text{tot}}/Z_\tau$, where Z_{EHD} and Z_τ are determined by Eqs. (6a), (6b), and (7).

Note that the thickness of the cathode sheath of a glow discharge is on the order of a few dozen mean free paths. Therefore, only a very thin portion of the laminar sublayer at the cathode would be directly affected. If the cathode is positioned downstream of the anode, the gas in this very thin layer at the cathode would experience ion wind forces directed both toward the surface and in the direction of the flow. What effect these forces would have on flow behavior, such as turbulent transition and heat transfer, remains to be studied.

In assessing ion wind effects, it is important to include the inevitable Joule heating. The ratio of Joule and viscous dissipation rates is

$$Z_\varepsilon = \frac{en_+V_{\text{dr}}^+\Delta\varphi}{\tau u'} = Z_\tau\frac{V_{\text{dr}}^+}{u'} \tag{12}$$

where V_{dr}^+ is the ion drift velocity. In the cathode sheath, where the electric field is extremely strong, ion drift velocity is very high, about $(5–10) \times 10^3$ m/s. Because u' is only several meters a second, Eq. (12) shows that the heating effect in the cathode sheath exceeds the ion wind effect by three orders of magnitude. Thermal expansion would push the gas from the wall, thus opposing the cathode-directed ion wind force. The heating would also increase viscosity. Additionally, heating occurs not only in the sheath, but also in the quasi-neutral plasma region of the discharge, while ion wind is confined to the space-charge region. Thus, even if the ion wind force can affect the viscous boundary layer, its action may be accompanied by the strong heating generated by the same electric discharge. With regard to the experiments[37,38] where EHD (ion wind) effects of surface glowlike discharges with dielectric barrier on low-speed flows have been demonstrated, it would be interesting to further investigate roles (if any) of viscous and thermal effects vs the EHD action on the inviscid low-speed core flow.

C. Basic Analysis of Magnetohydrodynamic Flow Control

To estimate MHD effects in relatively cold hypersonic flow and boundary layer, Eq. (5) should be analyzed jointly with other appropriate gasdynamic and plasma kinetic equations. The current density can be related to the values of electric and magnetic fields through the generalized Ohm law that is a consequence of Eqs. (1–4)[41]:

$$\boldsymbol{j} = \sigma\boldsymbol{E}^* + (\Omega_e/B)\boldsymbol{j}\times\boldsymbol{B} + \left(\Omega_e\Omega_i/B^2\right)(\boldsymbol{j}\times\boldsymbol{B})\times\boldsymbol{B} \tag{13}$$

where $\boldsymbol{E}^* = \boldsymbol{E} + \boldsymbol{u}\times\boldsymbol{B}$ is the electric field in the reference frame moving with the gas, and Ω_e and Ω_i are the electron and ion Hall parameters,

$$\Omega_e = \frac{eB}{mk_{\text{en}}n}, \qquad \Omega_i = \frac{eB}{M_nk_{n+}n} \tag{14}$$

The second term on the right-hand side of Eq. (13) represents the Hall effect, and the third term, nonlinear with respect to B, represents the ion slip. In the analysis, we will disregard negative ions and also assume quasi-neutrality: $n_e = n_+ \gg n_-$.

The MHD interaction parameter, also referred to as the Stuart number S, is the ratio of ponderomotive (Ampere) and inertia forces. With ion slip correction,

$$S = \frac{\sigma B^2L}{(1+\Omega_e\Omega_i)\rho u} \tag{15}$$

where L is the length of the MHD region. When ion slip is small ($\Omega_e\Omega_i \ll 1$), the Stuart number increases with magnetic field as B^2. However, at very strong magnetic fields and in low-density gases, when $\Omega_e\Omega_i \gg 1$, the interaction parameter reaches its asymptotic value independently of B:

$$S \to (L/u)k_{n+}n_+ \tag{16}$$

The physical meaning of Eq. (16) is that the maximum ion momentum change occurs when they are essentially stopped by the strong transverse magnetic field, and then momentum transfer from the ions to the gas is limited by the number of collisions of a neutral molecule with ions. Indeed, the right-hand side of Eq. (16) is simply the ratio of the flow residence time in the MHD region to the mean time for a molecule to collide with an ion.

As discussed in our earlier work,[16–18,22–24,26–28] at flight Mach numbers up to about Mach 12, thermal ionization even behind shocks cannot provide an adequate electrical conductivity for MHD flow control and power generation devices. (Above Mach 12, one might achieve adequate ionization near stagnation zones and in the boundary layers, but adequate ionization will not exist in the inviscid flow of slender bodies for Mach numbers much higher than 12.) The ionization must be created and sustained artificially, and the need to spend power on ionization severely limits performance of hypersonic MHD devices.[16–18,22–24,26–28] Indeed, the work done on an electron by the induced Faraday electric field during the electron's lifetime with respect to dissociative recombination with ions is

$$\varepsilon = eEV_{\text{dr}}^e\frac{1}{\beta n_+} = \frac{(eE)^2}{mk_{\text{en}}\beta nn_e} = \frac{(ekuB)^2}{mk_{\text{en}}\beta nn_e} \tag{17}$$

where k is the load factor, $E = kuB$ is the induced electric field, $V_{\text{dr}}^e = eE/mk_{\text{en}}n$ is the electron drift velocity, and β is the dissociative recombination rate constant. Although in the general problem of MHD flow control one might also be interested in the case where the device is not self-powered, self-powered MHD devices are obviously attractive, because they would not require any onboard power input. In this paper, we limit our analysis to self-powered MHD devices. For efficient self-powered operation of the MHD device, ε must be substantially larger than the energy cost W_i of a newly produced electron. Specifically, the ratio

$$\zeta \equiv \frac{W_i}{\varepsilon} = \frac{mk_{\text{en}}\beta nn_eW_i}{(ekuB)^2} \tag{18}$$

must be limited to a number less than 1. This obviously limits the electron density n_e and the conductivity:

$$\sigma = \frac{e^2 n_e}{m k_{\text{en}} n} = \frac{\zeta (e^2 k u B)^2}{(m k_{\text{en}} n)^2 \beta W_i} \tag{19}$$

The maximum interaction parameter per unit length is then

$$\frac{S}{L} = \frac{\zeta}{\beta W_i} \times \left(\frac{e^2 k M_n}{k_{\text{en}} m}\right)^2 \times \frac{B^4}{1 + M_n e^2 B^2 \big/ m k_{\text{en}} k_{n+} \rho^2} \times \frac{u}{\rho^3} \tag{20}$$

Hypersonic MHD devices would operate downstream of one or more oblique shocks, and it is convenient to express the interaction parameter in terms of flight velocity, Mach number, and dynamic pressure. Assuming that the MHD device is located downstream of a single oblique shock with flow turning angle θ, we express the density and velocity in terms of the freestream parameters M, u_∞, ρ_∞ with approximate formulas that can be easily derived for oblique shocks with small turning angles:

$$\rho = \frac{\rho_\infty}{f}, \qquad \frac{u}{\rho^3} = \frac{u_\infty}{\rho_\infty^3} \times \frac{f^4}{g}$$

$$f(M, \theta) = \frac{\gamma - 1}{\gamma + 1} + \frac{32}{(\gamma + 1)\left[(\gamma + 1) M \tan\theta + \sqrt{(\gamma + 1)^2 M^2 \tan^2\theta + 16}\right]^2}$$

$$g(M, \theta) = 1 - \frac{4 M \tan\theta}{(\gamma + 1) M \tan\theta + \sqrt{(\gamma + 1)^2 M^2 \tan^2\theta + 16}} \tag{21}$$

With Eq. (21), and expressing the freestream density in terms of dynamic pressure q and velocity, $\rho_\infty = 2q/u_\infty^2$, we obtain the final expression for the maximum Stuart number per unit length:

$$\frac{S}{L} = \left(\frac{e^2 k M_n}{k_{\text{en}} m}\right)^2 \times \frac{\zeta f^4 B^4 u_\infty^7}{8 g \beta W_i q^3} \times \left(1 + \frac{f^2 e^2 M_n B^2 u_\infty^4}{4 k_{\text{en}} k_{n+} q^2}\right)^{-1} \tag{22}$$

MHD performance as expressed by Eq. (22) is inversely proportional to the energy cost of producing an electron, W_i. Thus, minimization of W_i is critical. As shown in our earlier work,[16,18,26,28,32–34] dc, rf, and microwave methods of plasma generation have unacceptably high ionization cost, $W_i \sim 10^4$ eV. Electron beams represent the most efficient nonequilibrium method of ionization,[16,28,31,33] with $W_i = 34$ eV, and the concept of cold-air hypersonic MHD devices with ionization by electron beams was suggested and developed in our earlier work.[16–28] In what follows, we will assume that ionization is done by electron beams, with $W_i = 34$ eV, and that ζ is limited to 0.3.

Maximum MHD interaction parameter (22) increases very rapidly [especially if the ion slip, represented by the last factor in Eq. (22), is not significant] with increasing magnetic field and flight speed, and with decreasing dynamic pressure. The very sharp u_∞^7 dependence is due to both increase in the Faraday emf with flow velocity and to the decrease in gas density at constant q. Figure 1 shows S/L calculated with Eq. (22) vs flight Mach number at four different magnetic field strengths and two values of flight dynamic pressure. The load factor value was constant at $k = 0.5$.

At low gas density and strong B field, which favor MHD performance, the Hall effect becomes very significant. If the Hall current is allowed to flow, the effective conductivity is reduced by the factor $1 + \Omega_e^2$, and the MHD performance decreases. In Faraday MHD devices, Hall current is eliminated by segmenting electrodes.[42] However, as the longitudinal Hall electric field increases, arcing between the electrode segments can occur.[43] The arcing would essentially result in a continuous-electrode Faraday device, with dramatic reduction in performance.

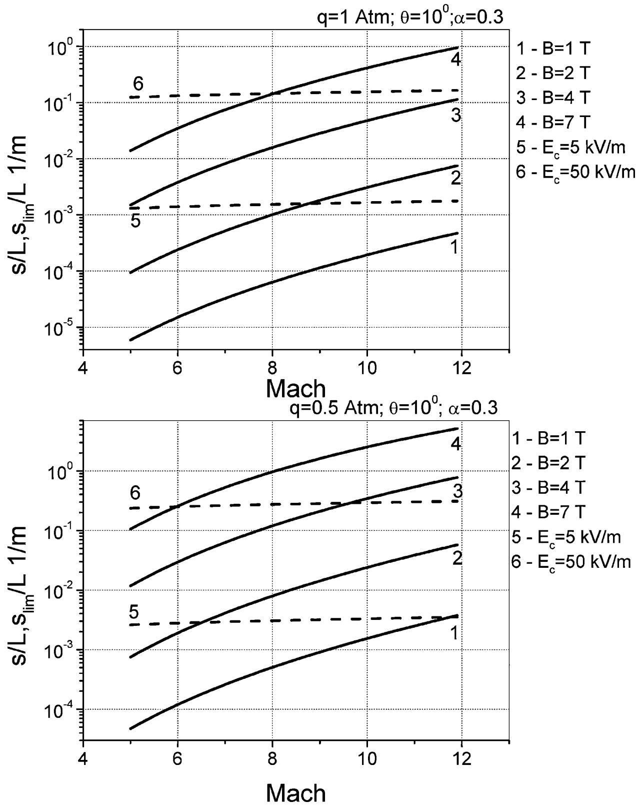

Fig. 1 Maximum MHD interaction parameter per unit length vs flight Mach number: solid lines, interaction parameter at different values of magnetic field, with no constraint on Hall field; dashed lines, upper limit of interaction parameter imposed by constraint on maximum allowed Hall field.

Denoting the value of the Hall field corresponding to the arcing threshold as E_c, an additional constraint in assessing the maximum performance is

$$E_c = (1 - k)\Omega_e u B = \frac{(1 - k) e^2 M_n u B^2}{k_{\text{en}} m \rho} \tag{23}$$

This condition limits the allowed B field at high flow velocity and low gas density. With this constraint, the upper limit for the interaction parameter per unit length becomes

$$\frac{S_{\text{lim}}}{L} = \frac{\zeta g e^2 E_c^2 u_\infty}{2 \beta W_i q}\left(1 + \frac{g e E_c u_\infty}{2(1 - k) k_{n+} q}\right)^{-1} \tag{24}$$

This formula does not explicitly depend on the B field and has a weak dependence on flight conditions because, at each flight regime, the B field is adjusted to satisfy Eq. (23).

Figure 1 shows the Hall field-limited interaction parameter of Eq. (24) at two values of E_c. Although the performance is quite good at $E_c = 50$ kV/m, it is unacceptably low with $E_c = 5$ kV/m. Therefore, determining the threshold field for intersegment arcing is critical for assessing performance of hypersonic MHD devices.

The intersegment arcing in conventional high-temperature MHD generators with thermal ionization was extensively studied both theoretically[42,44–46] and experimentally.[47,48] Computational study by Oliver[45] established 40 V as the intersegment potential drop corresponding to the onset of arcing, and experiments[48] gave the range 40–100 V. With centimeter-scale electrode width and intersegment gap, this would correspond to the longitudinal field of 50 V/cm or so. However, experimental[47,48] and theoretical[44,46] studies of this thermally induced arcing found that the arcing threshold increases with increasing magnetic field and decreasing electrode surface temperature. Qualitatively, this can be explained by the reduction in electrical conductivity in the boundary layer as the wall gets colder and by the effective boundary-layer conductivity reduction as $(1+\Omega_e^2)^{-1}$. Thus, even in conventional MHD devices with thermal ionization, E_c can be substantially higher than 50 V/cm.

More important, the operating conditions and the ionization mechanism in cold-air hypersonic MHD devices differ dramatically from those in conventional thermal systems. In on-ramp MHD shock control and power generation devices,[17,27] ionization ($n_e \sim 10^{12}$ cm^{-3}, $\sigma \approx 0.5$ mho/m) is sustained by electron beams. The rate of ionization by plasma electrons is very low,[16–18] because the ratio of effective electric field strength to the gas number density, $E_{\rm eff}/n \approx 10^{-16}$ V $\cdot$ cm^2, both in the core flow and in the boundary layer, results in low electron temperature. Because the gas temperature in both core flow and, with proper active wall cooling, near electrodes is below 1000 K, thermal ionization is also negligible. Therefore, electron-beam-sustained plasmas in hypersonic MHD devices should have higher thresholds of ionization and thermal instabilities than conventional thermally ionized plasma. We emphasize that the intersegment arcing in cold-air MHD devices with electron-beam-controlled ionization was never studied, and it should be studied in the future because of the critical importance of E_c for the performance of those devices.

The analysis in the preceding paragraphs of this subsection so far has been focused on MHD interaction parameters in the core flow. Similarly to the EHD analysis in Sec. II.B, one can define an MHD interaction parameter with respect to shear stress at the wall:

$$S_\tau = \sigma B^2 L/\rho \boldsymbol{u}' \tag{25}$$

where $\boldsymbol{u}'$ is the friction velocity defined by Eq. (8). If, for rough estimates, we assume that the conductivity σ and the density ρ near the wall are equal to those in the core flow (this can be ensured by a proper wall cooling and by contouring the profiles of ionizing electron beams), then from Eqs. (8–10) and (25) we obtain

$$S_\tau = \sqrt{2/c_f} \times \sigma B^2 L/\rho u = \sqrt{2/c_f} \times S \tag{26}$$

Therefore, in the range $Re_x^* = 10^5$–10^7, the MHD interaction parameter with respect to wall shear stress greatly exceeds S: $S_\tau \approx 30S$. This may have interesting implications for wall friction and transition control.

Of course, MHD effects on the boundary layer would be quite complex. First, if the load factor k is not close to 1 or 0, then the Joule heating is characterized by the same interaction parameters (15) and (25), and the heating effects should be comparable to those of ponderomotive $\boldsymbol{j}\times\boldsymbol{B}$ forces both in the core flow and near the wall. Second, if the MHD region extends into the core flow, the changes in the core flow would also affect the boundary layer. Thus, evaluation of MHD effects on the boundary layer requires a fully coupled analysis.

III. Electrodeless Magnetohydrodynamic Flow Control: A Magnetothermal Funnel

Because electrode-related problems like intersegment arcing can potentially reduce performance of MHD flow control devices, it is interesting to consider whether MHD flow turning or compression can be accomplished without electrodes.

Using one of the Maxwell equations,

$$\nabla \times \boldsymbol{B} = \mu_0 \boldsymbol{j} \tag{27}$$

and the vector identity

$$\tfrac{1}{2}\nabla B^2 = (\boldsymbol{B}\cdot\nabla)\boldsymbol{B} + \boldsymbol{B}\times(\nabla\times\boldsymbol{B}) \tag{28}$$

we obtain from Eq. (5)

$$\rho\frac{\mathrm{d}\boldsymbol{u}}{\mathrm{d}t} = -\nabla p + e(n_+ - n_- - n_e)\boldsymbol{E} + \frac{1}{\mu_0}(\boldsymbol{B}\cdot\nabla)\boldsymbol{B} - \nabla\frac{B^2}{2\mu_0} + \mu\Delta\boldsymbol{u}$$
$$= -\nabla\left(p + \frac{B^2}{2\mu_0}\right) + \frac{1}{\mu_0}(\boldsymbol{B}\cdot\nabla)\boldsymbol{B} + e(n_+ - n_- - n_e)\boldsymbol{E} + \mu\Delta\boldsymbol{u} \tag{29}$$

Thus, magnetic field energy density, $B^2/2\mu_0$, acts as an additional pressure. The term $1/\mu_0(\boldsymbol{B}\cdot\nabla)\boldsymbol{B}$ can be interpreted as tension of magnetic field lines due to their curvature. These ponderomotive forces are successfully used for containment of fully ionized plasmas in fusion devices.

With $B = 1$ T, the magnetic pressure is about 8 atm, and significant MHD flow turning and compression effects might be expected in hypersonic flow. However, practical applications of the magnetic ponderomotive flow control would be hampered by low ionization level. Indeed, with the conductivity of only 0.1–1 mho/m typical for MHD devices with ionization by electron beams, $Re_M = \mu_0\sigma u L \ll 1$ and the magnetic field is not "frozen" into the plasma. Therefore, ponderomotive forces depend on the conductivity, and their relative strength is characterized by the Stuart number S that, as shown in the preceding section, is also less than 1 for an MHD region of a few meters in length. Note the important difference between electric and magnetic pressures in weakly ionized plasmas. Whereas the electric pressure can fully act on even weakly ionized gases (see Sec. II.B), the magnetic pressure cannot be fully exerted on weakly ionized, low-conductivity media unless the flow velocity and/or the length scale are extremely large.

Consider a sample case of electrodeless MHD flow control, illustrated in Fig. 2. Gas flows into a cylindrical duct (inlet), and magnetic field lines are coming out of the duct in a pattern similar to that near the edge of a solenoid. Ionizing electron beams form an annular ring coaxial with and adjacent to the duct wall and are injected upstream, along B field lines. With the plasma moving across the nonuniform magnetic field, induced electric currents form circles coaxial with the inlet. The resulting $\boldsymbol{j}\times\boldsymbol{B}$ forces decelerate and compress the flow. Additionally, gas heating by the induced currents creates a reduced-density region around and upstream of the inlet, deflecting streamlines and causing an increase in compression and mass flow rate into the duct. Thus, both $\boldsymbol{j}\times\boldsymbol{B}$ forces and heating create what may be called a magnetothermal funnel.

The calculations were performed for freestream conditions corresponding to Mach 8 flight at the altitude $h = 30$ km, with static pressure and temperature of 1197 Pa and 226.5 K, respectively. The cylindrical inlet of radius, $r_{\rm inlet} = 1$ m, was positioned at axial location $z_{\rm inlet} = 2$ m. The model profile of a solenoid-like stationary magnetic field in the upstream region was

$$\boldsymbol{B} = [B_z(r,z), B_r(r,z), 0], \qquad B_z(r,z) = -\left[B_a^2(z,r) - B_r^2(r,z)\right]^{\frac{1}{2}}$$
$$B_a(z) = B_{a,\max}\exp[-(z - z_{\rm inlet})/4]$$
$$B_r(r,z) = B_a(z)(1 - \exp\{-[r/(0.5\cdot r_{\rm inlet})]\}) \tag{30}$$

with $B_{a,\max} = 7$ T.

The ionizing electron beams are injected in a 1-cm-wide ring around the inlet. The energy of beam electrons is $\varepsilon_b \approx 50$ keV, and their relaxation length under the conditions of this case is $L_R \approx 2.5$ m. The current density of the beam at the injection point is very high, $j_b \approx 72$ mA/cm^2, and the total power of the beam is

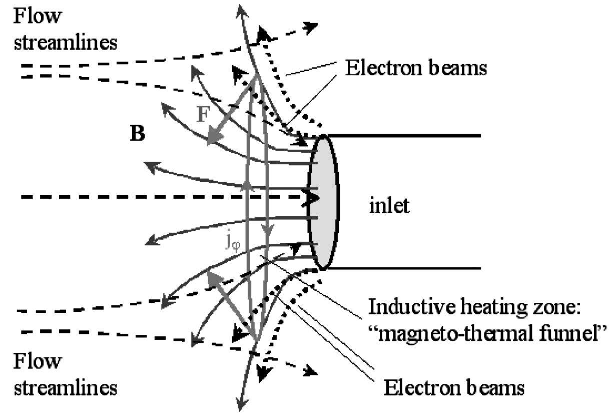

Fig. 2 Schematic illustration of the magnetothermal funnel concept.

$Q_b = 4.57$ MW. Power deposition by electron beams was modeled using a two-dimensional profile approximately following magnetic field lines:

$$q_b(z,r) = 3\times 10^6 \exp\{-[(z-0.7)^2/0.45^2 + (r-r_c)^2/r_{\mathrm{eff}}(z)^2]\}\ \mathrm{W/m^3}$$

$$r_c = 1.75\exp(-z/0.5) + 0.967$$

$$r_{\mathrm{eff}}(z) = 0.01 + 0.2\exp(-z/1.05) \tag{31}$$

where z and r are in meters. The profile of both beam-induced ionization rates corresponds to the beam power deposition profile:

$$q_i(z,r) \approx q_b(z,r)/(eW_i) \tag{32}$$

where $W_i = 34$ eV is the energy cost of ionization by high-energy beam electrons.

Generalized Ohm's law (13) in the case $\boldsymbol{u} = (u_z, u_r, 0)$, $\boldsymbol{B} = (B_z, B_r, 0)$, $\boldsymbol{j} = (0, 0, j_\varphi)$ is

$$j_\varphi = \frac{\sigma E_\varphi^*}{1+\Omega_e\Omega_i} = \frac{\sigma(u_z B_r - B_z u_r)}{1+\Omega_e\Omega_i} \tag{33}$$

This azimuthal current produces Joule heating of the gas:

$$Q_J = j_\varphi E_\varphi^* = \frac{\sigma(u_z B_r - B_z u_r)^2}{1+\Omega_e\Omega_i} \tag{34}$$

and $\boldsymbol{j}\times\boldsymbol{B}$ forces:

$$F_z = -j_\varphi B_r, \qquad F_r = j_\varphi B_z \tag{35}$$

The full set of Euler equations in cylindrical coordinates is

$$\frac{\partial}{\partial t}U + \frac{\partial}{\partial r}R + \frac{\partial}{\partial z}Z = H \tag{36}$$

$$U = \begin{Vmatrix} \rho \\ \rho u_r \\ \rho u_z \\ e_{\mathrm{tot}} \\ E_v \end{Vmatrix}, \qquad R = \begin{Vmatrix} \rho u_r \\ \rho u_r^2 + p \\ \rho u_r u_z \\ (e_{\mathrm{tot}}+p)u_r \\ E_v u_r \end{Vmatrix}, \qquad Z = \begin{Vmatrix} \rho u_z \\ \rho u_r u_z \\ \rho u_z^2 + p \\ (e_{\mathrm{tot}}+p)u_z \\ E_v u_z \end{Vmatrix}$$

$$H = -\frac{1}{r}\begin{Vmatrix} \rho u_r \\ \rho u_r^2 \\ \rho u_r u_z \\ (e_{\mathrm{tot}}+p)u_r \\ E_v u_r \end{Vmatrix} + \begin{Vmatrix} 0 \\ -j_\varphi B_r \\ j_\varphi B_z \\ Q \\ Q_v - Q_{\mathrm{VT}} \end{Vmatrix} \tag{37}$$

$$p = (\gamma - 1)\rho\varepsilon_{\mathrm{int}} \tag{38}$$

$$e_{\mathrm{tot}} = \rho\left[\varepsilon_{\mathrm{int}} + \left(u_r^2 + u_z^2\right)/2\right] \tag{39}$$

where ρ and p denote the gas density and pressure, respectively; u_r, u_z are the r and z velocity components; e_{tot} is the total energy (internal energy, excluding the energy of vibrational mode, plus kinetic energy) of the gas per unit volume; and $\varepsilon_{\mathrm{int}}$ is the internal energy (excluding the energy of vibrational mode) per unit mass.

The source term in the total energy equation is

$$Q = -Q_v + Q_{\mathrm{VT}} + q_b \tag{40}$$

where the vibrational excitation term Q_v can be expressed as a fraction η_v of the Joule heating rate: $Q_v = \eta_v j_\varphi^2/\sigma$. The fraction η_v is a function of the local reduced electric field $E_{\mathrm{eff}}/n = |u_z B_r - B_z u_r|/n$. The fraction η_v was taken from Ref. 49, where it was tabulated as a function of E/n on the basis of the solution of a Boltzmann kinetic equation for plasma electrons. The remaining energy addition and dissipation terms are

$$Q_{\mathrm{VT}} = \left[E_v - E_v^0(T)\right]\big/\tau_{\mathrm{VT}}(T) \tag{41}$$

where Q_{VT} is the heating rate per unit volume due to VT relaxation; and q_b is the power deposited per unit volume by the electron beam. Nonequilibrium and equilibrium vibrational energy was expressed through the respective temperatures by the Planck formula, and nitrogen vibrational relaxation time was taken as in Refs. 16–18.

The plasma was modeled as consisting of electrons and positive and negative ions, whose number densities n_e, n_+, n_- obey the quasi neutrality $n_+ \approx n_e + n_-$. The set of equations for kinetics of charge species, accounting for electron-beam-induced ionization rate (q_i term), ionization rate due to plasma electrons (with Townsend ionization coefficient α depending on the local reduced electric field, $E_{\mathrm{eff}}/n = |u_z B_r - B_z u_r|/n$), attachment of electrons to molecules with formation of negative ions (frequency ν_a), collisional detachment of electrons from negative ions (rate constant k_d), and electron–ion and ion–ion recombination (rate coefficients β and β_{ii}, respectively), is[16–18,33,36]

$$\frac{\partial n_e}{\partial t} + \operatorname{div}\boldsymbol{\Gamma}_e = \frac{\alpha|j_\varphi|}{e} + q_i + k_d N n_- - \nu_a n_e - \beta n_+ n_e$$

$$\frac{\partial n_+}{\partial t} + \operatorname{div}\boldsymbol{\Gamma}_+ = \frac{\alpha|j_\varphi|}{e} + q_i - \beta_{ii} n_- n_+ - \beta n_+ n_e$$

$$\frac{\partial n_-}{\partial t} + \operatorname{div}\boldsymbol{\Gamma}_- = -k_d N n_- + \nu_a n_e - \beta_{ii} n_- n_+ \tag{42}$$

In the considered case, there are no drift fluxes along either z or r axes (only azimuthal current j_φ is present) and, therefore, the fluxes of charged species in the r–z plane can be written simply as $\boldsymbol{\Gamma}_{e,+,-}(r,z) = n_{e,+,-}(\tilde{u}_z \cdot \boldsymbol{i}_z + \tilde{u}_r \cdot \boldsymbol{i}_r)$, where $\boldsymbol{i}_{r,z}$ are the vectors of unit length in z and r directions and $\tilde{u}_{r,z}$ is the effective electron–ion velocity across the magnetic field taking into account ion slip[17,18]:

$$\tilde{u}_{r,z} = u_{r,z}/(1 + \Omega_e\Omega_+) \tag{43}$$

The initial conditions for plasma components are $n_{e,+,-}(r, z, t = 0) = 0$. The boundary conditions are

$$n_{e,+,-}(z=0,r,t) = n_{e,+,-}(z=z_{\max},r,t) = 0$$

$$n_{e,+,-}(z, r=r_{\max}, t) = 0, \qquad \mathrm{d}n_{e,+,-}(z, r=0, t)/\mathrm{d}r = 0 \tag{44}$$

Rate coefficients of electron–ion and ion–ion recombination, and of electron attachment and detachment processes, discussed in Refs. 16–18 and 31–34, were taken from Refs. 50 and 51. Because some of those rate coefficients depend on electron temperature T_e, it is important to calculate the electron temperature in the modeling. In our computations, electron temperature was determined from the tabulated data on electron diffusion and mobility coefficients of Ref. 49. In that paper, the diffusion and mobility coefficients are listed as functions of E/N, determined from experimental data and extrapolation based on solution of the Boltzmann kinetic equation for electrons in air.

Results of the calculations are shown in Figs. 3–10. Figure 3 depicts the magnetic field lines, and Fig. 4 shows the electron beam power deposition profile. The resulting profiles of electron density and azimuthal current are shown in Figs. 5 and 6. Figures 7–10 show the computed profiles of static and vibrational temperatures, gas density, and radial velocity. The formation of a magnetothermal funnel is clearly seen in the figures.

The overall performance of the funnel can be assessed by the mass flow rate and enthalpy flux into the inlet and by the total pressure

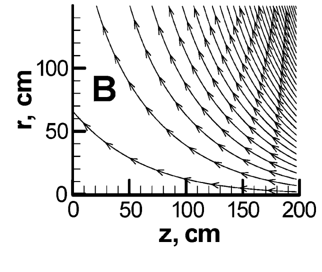

Fig. 3 Magnetic field lines in the computed case.

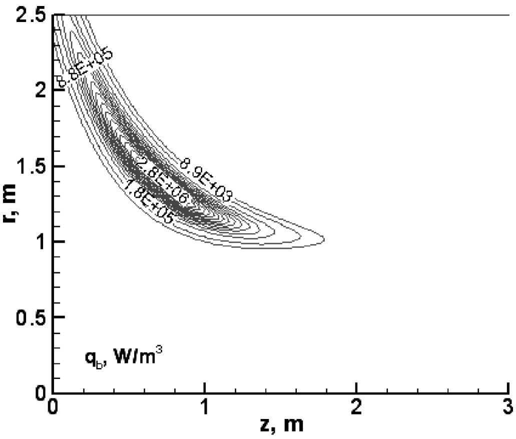

Fig. 4 Electron beam power deposition contour lines in the computed case.

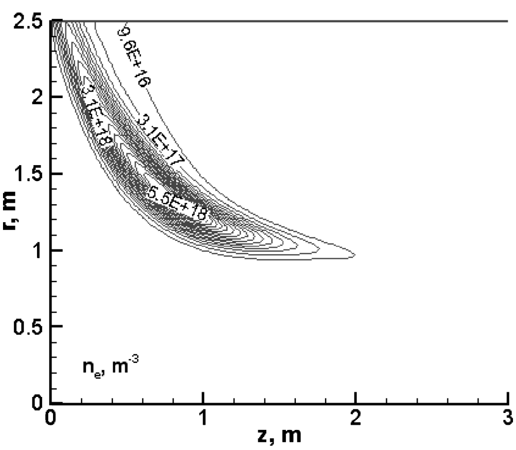

Fig. 5 Electron number density contours in the computed case.

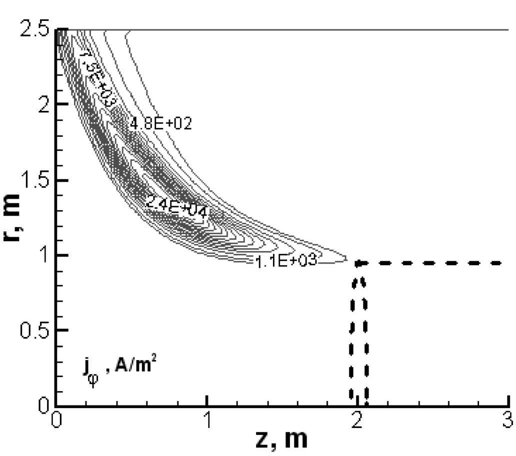

Fig. 6 Azimuthal current density contour lines in the computed case.

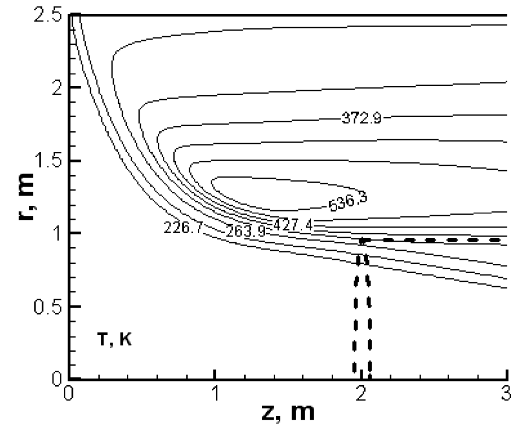

Fig. 7 Static temperature contours in the computed case.

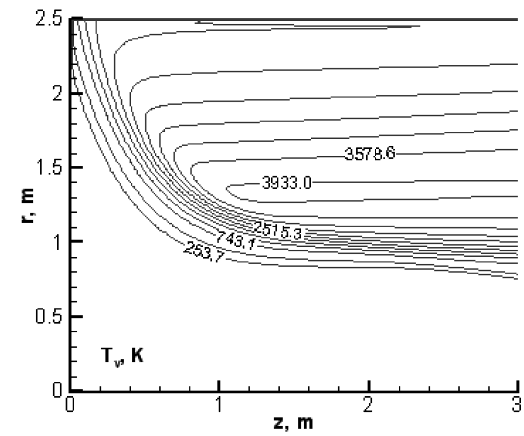

Fig. 8 Vibrational temperature contour lines in the computed case.

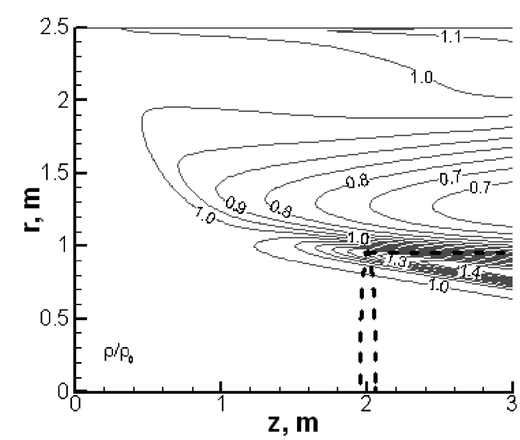

Fig. 9 Density contours in the computed case.

coefficient. Without ionization ($q_b = 0$), the mass flow and enthalpy flux into the inlet are the following:

$$\dot{m}_{z=z_{\text{inlet}}} = \int_0^{r_{\text{inlet}}} 2\pi r \rho(z, r) u_z \, \mathrm{d}r = 139.6 \text{ kg/s}$$

$$\dot{H}_{z=z_{\text{inlet}}} = \int_0^{r_{\text{inlet}}} 2\pi r \rho(z, r) u_z \left[\frac{\gamma p}{(\gamma - 1)\rho} + 0.5\left(u_z^2 + u_r^2\right) \right] \mathrm{d}r$$

$$= 438.5 \text{ MW}$$

The total pressure coefficient, that is, the total pressure averaged over the inlet cross section divided by the freestream total pressure, is $\langle p_{\text{tot}} \rangle / p_{\text{tot},0} = 1$. When the electron beam is turned on, but in the absence of any magnetic field ($B = 0$, $q_b \neq 0$), gas heating by the beam and streamline deflection result in a barely noticeable increase in mass and enthalpy fluxes and a slight decrease in total pressure: $\dot{m}_{z=z_{\text{inlet}}} = 139.9$ kg/s, $\dot{H}_{z=z_{\text{inlet}}} = 439.4$ MW, $\langle p_{\text{tot}} \rangle / p_{\text{tot},0} = 0.997$. With both ionization and magnetic field on ($\boldsymbol{B} = \boldsymbol{B}(r, z)$, $q_b \neq 0$), the increased mass and enthalpy fluxes and the decreased total pressure coefficient are $\dot{m}_{z=z_{\text{inlet}}} = 146$ kg/s, $\dot{H}_{z=z_{\text{inlet}}} = 457.8$ MW, $\langle p_{\text{tot}} \rangle / p_{\text{tot},0} = 0.93$. The maximum flow turning induced in the flowfield is about 2.5 deg.

The computations were performed with the second-order MacCormack method[52] on a rectangular 310×250 grid. Computations with a finer grid, 465×375, show that the mass and enthalpy fluxes and the total pressure are within 0.1% from those

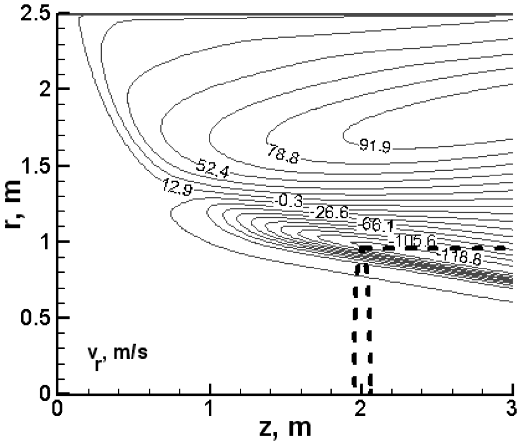

Fig. 10 Radial velocity contour lines in the computed case.

computed with the 310×250 grid, thus confirming the accuracy of computations.

Thus, the magnetothermal funnel can indeed increase mass capture and total enthalpy flux into the inlet. However, because of gas heating, the total pressure would decrease. In the sample case, the beam and magnetic field parameters were not optimized, and the effects are quite modest despite the very high current density of the beam. The mass flow rate increase can be made stronger by using stronger magnetic fields and higher beam currents. Practicality of this method of flow control, with advantages weighted against flaws (strong magnetic fields, high electron beam currents, and losses of total pressure), should be the a subject of a systems study.

IV. Conclusions

The principal difficulty in high-speed flow control using electric and magnetic fields is that the relatively cold gas has to be ionized in electric discharges or by electron beams, which requires large power inputs and results in low ionization fraction and electrical conductivity. The low ionization fraction means that, although electrons and ions can interact with electromagnetic fields, transfer of momentum and energy to or from the bulk neutral gas can be small compared with momentum and energy carried by the high-speed flow.

Even at the highest values of the electric field that can exist in cathode sheaths of electric discharges, EHD, or ion wind, effects in a single discharge can be of significance only in low-speed core flows or in a laminar sublayer of the boundary layer. Cumulative action of multi-element discharges would conceivably amplify the single-sheath effect. However, Joule heating can overshadow the cathode sheath ion wind effects.

Theoretical analysis of MHD flow control with electron beam ionization of hypersonic flow shows that the MHD interaction parameter is a steeply increasing function of magnetic field strength and the flow velocity. However, constraints imposed by arcing between electrode segments can reduce the performance and make the maximum interaction parameter virtually independent of Mach number. Thus, the value of critical Hall field corresponding to the onset of arcing between electrode segments is extremely important in designing and evaluating performance of hypersonic MHD devices, and the arcing instability should be investigated theoretically and experimentally.

Estimates of MHD interaction parameter with respect to shear stress show that the relative strength of MHD effects can be higher near the wall (in the boundary layer) than in the core flow, which may have implications for MHD boundary-layer and transition control. Overall, one of the qualitative conclusions from this work is that large-scale bulk MHD effects on the overall hypersonic flowfield are quite difficult (although not impossible) to achieve, whereas small and/or localized MHD effects such as those for small-angle flow turning or boundary-layer control may be useful for significant flowfield manipulation.

In this paper, we also suggested a magnetothermal funnel concept that would accomplish and electrodeless MHD turning and compression of high-speed flows. Computations of a sample case demonstrate that the turning and compression of hypersonic flow ionized by electron beams can be achieved; however, the effect is relatively modest due to low ionization level.

Acknowledgments

The work was supported by the Air Force Office of Scientific Research and, in part, by Boeing Phantom Works (St. Louis, Missouri) through Plasma Tec, Inc. The authors express their gratitude to Philip Smereczniak and Joseph Silkey of Boeing Phantom Works and to Graham Candler of the University of Minnesota for valuable discussions and advice.

References

[1]Fraishtadt, V. L., Kuranov, A. L., and Sheikin, E. G., "Use of MHD Systems in Hypersonic Aircraft," *Technical Physics*, Vol. 43, No. 11, 1998, pp. 1309–1313.

[2]Gurijanov, E. P., and Harsha, P. T., "AJAX: New Directions in Hypersonic Technology," AIAA Paper 96-4609, Nov. 1996.

[3]Bityurin, V. A., Lineberry, J. T., Potebnia, V. G., Alferov, V. I., Kuranov, A. L., and Sheikin, E. G., "Assessment of Hypersonic MHD Concepts," AIAA Paper 97-2323, June 1997.

[4]Bityurin, V. A., Klimov, A. I., Leonov, S. B., Bocharov, A. N., and Lineberry, J. T., "Assessment of a Concept of Advanced Flow/Flight Control for Hypersonic Flights in Atmosphere," AIAA Paper 99-4820, Nov. 1999.

[5]Brichkin, D. I., Kuranov, A. L., and Sheikin, E. G., "MHD Technology for Scramjet Control," AIAA Paper 98-1642, April 1998.

[6]Kuranov, A. L., and Sheikin, E. G., "The Potential of MHD Control for Improving Scramjet Performance," AIAA Paper 99-3535, June 1999.

[7]Brichkin, D. I., Kuranov, A. L., and Sheikin, E. G., "The Potentialities of MHD Control for Improving Scramjet Performance," AIAA Paper 99-4969, Nov. 1999.

[8]Kuranov, A. L., and Sheikin, E. G., "MHD Control on Hypersonic Aircraft Under AJAX Concept: Possibilities of MHD Generator," AIAA Paper 2002-0490, Jan. 2002.

[9]Chase, R. L., Mehta, U. B., Bogdanoff, D. W., Park, C., Lawrence, S., Aftosmis, M., Macheret, S. O., and Shneider, M. N., "Comments on an MHD Energy Bypass Engine Powered Spaceliner," AIAA Paper 99-4965, Nov. 1999.

[10]Park, C., Mehta, U. B., and Bogdanoff, D. W., "Real Gas Calculation of MHD-Bypass Scramjet Performance," AIAA Paper 2000-3702, July 2000.

[11]Golovachev, Yu. P., and Sushikh, S. Yu., "Supersonic Air-Scoop Flows of a Weakly Ionized Gas in External Electromagnetic Field," *Technical Physics*, Vol. 45, No. 2, 2000, p. 168.

[12]Golovachev, Yu. P., Sushikh, S. Yu., and Van Wie, D., "Numerical Simulation of MGD Flows in Supersonic Media," AIAA Paper 2000-2666, June 2000.

[13]Vatazhin, A., Kopchenov, V., and Gouskov, O., "Some Estimations of Possibility to Use the MHD Control for Hypersonic Flow Deceleration," AIAA Paper 99-4972, Nov. 1999.

[14]Kopchenov, V., Vatazhin, A., and Gouskov, O., "Estimation of Possibility of Use of MHD Control in Scramjet," AIAA Paper 99-4971, Nov. 1999.

[15]Vatazhin, A., Kopchenov, V., and Gouskov, O., "Numerical Investigation of Hypersonic Inlets Control by Magnetic Field," *2nd Workshop on Magneto- and Plasma Aerodynamics in Aerospace Applications*, Inst. of High Temperatures, Russian Academy of Sciences, Moscow, 2000, pp. 56–63.

[16]Macheret, S. O., Shneider, M. N., Miles, R. B., and Lipinski, R. J., "Electron Beam Generated Plasmas in Hypersonic Magnetohydrodynamic Channels," *AIAA Journal*, 2001, Vol. 39, No. 6, pp. 1127–1136.

[17]Macheret, S. O., Shneider, M. N., and Miles, R. B., "Magnetohydrodynamic Control of Hypersonic Flow and Scramjet Inlets Using Electron Beam Ionization," *AIAA Journal*, Vol. 40, No. 1, 2002, pp. 74–81.

[18]Macheret, S. O., Shneider, M. N., and Miles, R. B., "MHD Power Extraction from Cold Hypersonic Air Flow with External Ionizers," *Journal of Propulsion and Power*, Vol. 18, No. 2, 2002, pp. 424–431.

[19]Macheret, S. O., Miles, R. B., and Nelson, G. L., "Feasibility Study of a Hybrid MHD/Radiatively Driven Facility for Hypersonic Ground Testing," AIAA Paper 97-2429, June 1997.

[20]Macheret, S. O., Shneider, M. N., Miles, R. B., Lipinski, R. J., and Nelson, G. L., "MHD Acceleration of Supersonic Air Flows Using Electron Beam-Enhanced Conductivity," AIAA Paper 98-2922, June 1998.

[21]Shneider, M. N., Macheret, S. O., and Miles, R. B., "Electrode Sheaths and Boundary Layers in Hypersonic MHD Channels," AIAA Paper 99-3532, June 1999.

[22]Macheret, S. O., Shneider, M. N., and Miles, R. B., “Electron Beam Generated Plasmas in Hypersonic MHD Channels,” AIAA Paper 99-3635, June 1999.

[23]Macheret, S. O., Shneider, M. N., and Miles, R. B., “MHD Power Extraction from Cold Hypersonic Air Flow with External Ionizers,” AIAA Paper 99-4800, Nov. 1999.

[24]Macheret, S. O., Ionikh, Y. Z., Martinelli, L., Barker, P. F., and Miles, R. B., “External Control of Plasmas for High-Speed Aerodynamics,” AIAA Paper 99-4853, Nov. 1999.

[25]Simmons, G. A., Nelson, G. L., Cambier, J.-L., Macheret, S. O., Shneider, M. N., Lipinski, R. J., and Reed, K. W., “Electron Beam Driven MHD for the RDHWT/MARIAH II Hypersonic Wind Tunnel,” AIAA Paper 2000-2277, June 2000.

[26]Macheret, S. O., Shneider, M. N., and Miles, R. B., “Potential Performance of Supersonic MHD Power Generators,” AIAA Paper 2001-0795, Jan. 2001.

[27]Macheret, S. O., Shneider, M. N., and Miles, R. B., “External Supersonic Flow and Scramjet Inlet Control by MHD with Electron Beam Ionization,” AIAA Paper 2001-0492, Jan. 2001.

[28]Macheret, S. O., Shneider, M. N., and Miles, R. B., “Energy-Efficient Generation of Nonequilibrium Plasmas and Their Applications to Hypersonic MHD Systems,” AIAA Paper 2001-2880, June 2001.

[29]Girgis, I., Shneider, M., Macheret, S., Brown, G., and Miles, R., “Creation of Steering Moments in Supersonic Flow by Off-Axis Plasma Heat Addition,” AIAA Paper 2002-0129, Jan. 2002.

[30]Miles, R., Martinelli, L., Macheret, S., Shneider, M., Girgis, I., Zaidi, S., Mansfield, D., Siclari, M., Smereczniak, O., Kashuba, R., and Vogel, P., “Suppression of Sonic Boom by Dynamic Off-Body Energy Addition and Shape Optimization,” AIAA Paper 2002-0150, Jan. 2002.

[31]Macheret, S. O., Shneider, M. N., and Miles, R. B., “Modeling of Discharges Generated by Electron Beams in Dense Gases: Fountain and Thunderstorm Regimes,” *Physics of Plasmas*, Vol. 8, No. 5, 2001, pp. 1518–1528.

[32]Macheret, S. O., Shneider, M. N., and Miles, R. B., “Modeling of Air Plasma Generation by Repetitive High-Voltage Nanosecond Pulses,” *IEEE Transactions on Plasma Science*, Vol. 30, No. 3, 2002, pp. 1301–1314.

[33]Macheret, S. O., Shneider, M. N., and Miles, R. B., “Modeling of Air Plasma Generation by Electron Beams and High-Voltage Pulses,” AIAA Paper 2000-2569, June 2000.

[34]Macheret, S. O., Shneider, M. N., and Miles, R. B., “Modeling of Plasma Generation in Repetitive Ultra-Short High-Power DC, Microwave, and Laser Pulses,” AIAA Paper 2001-2940, June 2001.

[35]El-Khabiry, S., and Colver, G. M., “Drag Reduction by DC Corona Discharge Along an Electrically Conductive Flat Plate for Small Reynolds Number Flow,” *Physics of Fluids*, Vol. 9, No. 3, 1997, pp. 587–599.

[36]Raizer, Yu. P., *Physics of Gas Discharges*, Springer, Berlin, 1991, Chaps. 14, 17.

[37]Roth, J. R., Sherman, D. M., and Wilkinson, S. P., “Boundary Layer Flow Control with a One Atmosphere Uniform Glow Discharge Surface Plasma,” AIAA Paper 98-0328, Jan. 1998.

[38]Roth, J., Sin, H., Madhan, R., and Wilkinson, S., “Flow Re-Attachment and Acceleration by Paraelectric and Peristaltic Electrohydrodynamic (EHD) Effects,” AIAA Paper 2003-0531, Jan. 2003.

[39]Yu, L., Laux, C. O., Packan, D. M., and Kruger, C. H., “Direct-Current Glow Discharges in Atmospheric Pressure Air Plasmas,” *Journal of Applied Physics*, Vol. 91, No. 5, 2002, pp. 2678–2686.

[40]Henoch, C., and Stace, J., “Experimental Investigation of a Salt Water Turbulent Boundary Layer Modified by an Applied Streamwise Magnetohydrodynamic Body Force,” *Physics of Fluids*, Vol. 7, No. 6, 1995, pp. 1371–1383.

[41]Anderson, J. D., Jr., *Hypersonic and High Temperature Gas Dynamics*, McGraw–Hill, New York, 1988, pp. 286, 287.

[42]Rosa, R. J., *Magnetohydrodynamic Energy Conversion*, McGraw–Hill, New York, 1968, Chaps. 3, 4.

[43]Cowling, T. G., *Magnetohydrodynamics*, Interscience, New York, 1957, Chap. 3.

[44]Nedospasov, A. V., and Khait, V. D., *Fundamentals of Physics of Processes in Devices with Low Temperature Plasmas* (“*Osnovy Fiziki Protsessov v Ustroistvakh s Nizkotemperaturnoi Plazmoi*”), Energoatomizdat, Moscow, 1991, Chap. 6.

[45]Oliver, D. A., “Numerical Simulations of Interelectrode Arcing in MHD Generators,” *Proceedings of 14th Symposium on Engineering Aspects of MHD*, Univ. of Tennessee Space Inst., Tullahoma, TN, 1974, pp. 8.6.1–8.6.7.

[46]Nedospasov, A. V., Paramonov, A. A., and Khait, V. D., “Theory of Arcing Between Electrodes of MHD Generator,” *Proceedings of the 8th International Conference on MHD Energy Conversion*, Vol. 1, Inst. of High Temperatures, Russian Academy of Sciences, Moscow, 1983, pp. 264–276.

[47]Heydt, R. P., and Eustis, R. H., “Experimental Studies of Arcing Threshold in MHD Generators at High Hall Parameters,” *Proceedings of 21st Symposium on Engineering Aspects of MHD*, Supplemental Vol., Argonne National Lab., Argonne, IL, 1983, pp. 11–15.

[48]Zalkind, V. I., Kirillov, V. V., Tikhotskii, A. S., Uspenskaia, G. L., Burenkov, D. K., and Strekalov, N. B., “An Experimental Investigation of the Interelectrode Breakdown in MHD Channels,” *Teplofizika Vysokikh Temperatur (High Temperature)*, Vol. 19, No. 5, 1981, pp. 1050–1060.

[49]Aleksandrov, N. L., Vysikailo, F. I., Islamov, R. Sh., Kochetov, I. V., Napartovich, A. P., and Pevgov, V. G., “Electron Distribution Function in 4:1 N_2-O_2 Mixture,” *High Temperature*, Vol. 19, No. 1, 1981, pp. 17–21.

[50]Kossyi, I. A., Kostinsky, A. Yu., Matveyev, A. A., and Silakov, V. P., “Kinetic Scheme of the Non-Equilibrium Discharge in Nitrogen–Oxygen Mixtures,” *Plasma Sources Science and Technology*, Vol. 1, No. 3, 1992, pp. 207–220.

[51]Bazelyan, E. M., and Raizer, Yu. P., *Spark Discharge*, CRC Press, Boca Raton, FL, 1997, Chap. 2.

[52]Anderson, D. A., Tannehill, J. C., and Pletcher, R. H., *Computational Fluid Mechanics and Heat Transfer*, Hemisphere, New York, 1984, Chap. 4.

G. Candler
Associate Editor